Available online at www.sciencedirect.com
ScienceDirect
Journal of Solid State Chemistry 180 (2007) 995–1001
JOURNAL OF SOLID STATE CHEMISTRY
www.elsevier.com/locate/jssc

Crystal structures of $Na_{1/2}Ln_{1/2}TiO_3$ (*Ln*: La, Eu, Tb)

Rajeev Ranjan[a,b,*], Anatoliy Senyshyn[c,d], Hans Boysen[a], Carsten Baehtz[e], Friedrich Frey[a]

[a]*Department fur Geo-und Umweltwissenschaften, Sektion Kristallographie, Ludwig Maximilians Universität München, Am Coulombwall 1, 85747 Garching b. München, Germany*
[b]*School of Materials Science and Technology, Institute of Technology, Banaras Hindu University, Varanasi 221005, India*
[c]*Institute for Materials Science, Darmstadt University of Technology, Petersenstrasse 23, D-64287 Darmstadt, Germany*
[d]*Forschungsneutronenquelle Heinz Maier-Leibnitz (FRM II), Technische Universität München, Lichtenbergstrasse 1, 85747, Garching, München, Germany*
[e]*Hasylab/DESY, Notkestr. 85, 22607 Hamburg, Germany*

Received 18 November 2006; received in revised form 15 December 2006; accepted 24 December 2006
Available online 9 January 2007

Abstract

Neutron powder diffraction studies of $Na_{1/2}La_{1/2}TiO_3$ and $Na_{1/2}Tb_{1/2}TiO_3$, and a synchrotron X-ray powder diffraction study of $Na_{1/2}Eu_{1/2}TiO_3$ have been carried out. Rietveld refinement of the structures confirmed that $Na_{1/2}Eu_{1/2}TiO_3$ and $Na_{1/2}Tb_{1/2}TiO_3$ crystallizes in $GdFeO_3$ type of structure (space group *Pbnm*). The ambiguity in the literature regarding the crystal structure of $Na_{1/2}La_{1/2}TiO_3$ has been resolved and the correct space group is found to be $R\bar{3}c$. A detailed list of refined structural parameters of these compounds is presented for the first time.

Keywords: Perovskite; Titanates; Neutron diffraction; Quantum paraelectrics

1. Introduction

Perovskites with ABX_3 stoichiometry continue to attract wider interest because of their fascinating electrical, magnetic and optical properties [1–4]. Silicate perovskites constitute major part of the Earth lower mantle [1], and understanding of their phase transition behavior is of interest to seismology [5]. The simplest perovskite structure has cubic symmetry in the space group $Pm\bar{3}m$ with *A* occupying the 1*b* site at (0.5,0.5,0.5), *B* occupies 1*a* site at (0, 0, 0) and *X* occupies 3*d* site at (0,0,0.5). However, only a few limited numbers of the perovskites exhibit this simple structure type at ambient conditions. The vast majority exhibit slight distortion with respect to the cubic structure. These distortions are often a result of structural phase transition(s) that occur while cooling the material from high temperature. Most of these structural transitions involve tilting and distortions of the anion octahedra in different ways leading to variety of structures. The possible tilted perovskite structures have been classified systematically by Glazer [6,7]. In this scheme of structure analysis, a distorted perovskite structure is considered as a superposition of octahedral tilts (in-phase and out-of-phase) about the three pseudocubic axes. The in-phase (+) and the out-of-phase (−) tilts are associated with the irreducible representations, M_3^+ ($k = 1/2,1/2,0$) and R_4^+ ($k = 1/2, 1/2,1/2$), respectively, of the space group $Pm\bar{3}m$ [8].

In this paper we report the results of Rietveld refinement of the structures of three compounds $Na_{1/2}La_{1/2}TiO_3$ (NLT), $Na_{1/2}Tb_{1/2}TiO_3$ (NTT) and $Na_{1/2}Eu_{1/2}TiO_3$ (NET). Of these, NLT belongs to the Loparite family of minerals found in foidolites and aegirine-albite metasomatic rocks [9]. These compounds are also known to exhibit a not so well understood phenomenon of quantum paraelectricity at low temperatures (<50 K). The dielectric permittivity of the compounds exhibiting

*Corresponding author. Department fur Geo-und Umweltwissenschaften, Sektion Kristallographie, Ludwig Maximilians Universität München, Am Coulombwall 1, 85747 Garching b. München, Germany.
Tel.: 49 89 289 14018; fax: +49 89 289 14015.
E-mail address: rajeev.ranjan@physik.uni-muenchen.de (R. Ranjan).

0022-4596/$ - see front matter © 2007 Elsevier Inc. All rights reserved.
doi:10.1016/j.jssc.2006.12.030

quantum paraelectricity increases on cooling but saturates below a certain temperature T_a of the compound. It is believed that the zero point quantum fluctuations prevent freezing of a ferroelectric soft mode and stabilize the paraelectric phase below T_a [10]. Because of the comparatively high saturation temperature compared to other well-known quantum paraelectrics ($SrTiO_3$ [10] and $KTaO_3$ [11]) these compounds have also been termed as "high temperature quantum paraelectrics" [12,13].

Crystal structure plays an important role in determining the dielectric behavior of perovskites. For structures with weak distortion, the determination of the correct symmetry becomes a challenging task. In such a situation, neutron diffraction data is of particular importance since it can help to identify the correct structure among the competing structural models. We have recently demonstrated this aspect by identifying the structures of $Na_{1/2}Nd_{1/2}TiO_3$ (NNT), $Na_{1/2}Pr_{1/2}TiO_3$ (NPT) [14] and a series of solid solutions of $Na_{1/2}Pr_{1/2}TiO_3$–$SrTiO_3$ [15]. For NTT and NET, although orthorhombic structures in space group *Pbnm* have been proposed using laboratory X-ray diffraction data, no detailed structure refinement has been reported so far. Further, there are contradictory reports about the structure of NLT. While Sun et al. [12] have reported rhombohedral structure in space group$R\bar{3}c$, Mitchell and Chakhmouradian [16], and more recently Knapp and Woodward [17] have reported orthorhombic structure in space group *Pbnm*. The ambiguity in identifying the correct structural model arises from the fact that (1) the distortion of perovskite structure is weak and (2) the authors used X-ray diffraction data for structure analysis. As already mentioned, since primary cause of deviation from the cubic symmetry is tilting of the anion (oxygen in our case) octahedra, the intensities of the superlattice reflections due to octahedral tilts are relatively very weak in the X-ray diffraction patterns and may get lost in the background because of the weak scattering power of oxygen atoms for X-rays. In this work we have settled the structural controversy of NLT unambiguously by using neutron powder diffraction data. Neutron diffraction data has also been collected on NTT for a reliable determination of the oxygen positions and octahedral tilt angles. For NET, we have used high-resolution synchrotron XRD data because of the very large absorption cross section of Eu for thermal neutrons.

2. Experimental details

Specimens of NLT, NTT and NET were synthesized by conventional solid-state reaction method. Powders of Na_2CO_3, La_2O_3, Tb_4O_7, Eu_2O_3 and TiO_2, each of purity higher than 99.5%, were thoroughly mixed in stoichiometric ratio in a ball mill with agate jars and agate balls. Acetone was used as a mixing medium. The mixed powders were calcined at 1000 °C for 3 h and were cold compacted before sintering at 1300 °C in air for 3 h. The sintered powders were checked for their phase purity using laboratory powder X-ray diffraction (STOE). Neutron powder diffraction data were collected at powder diffractometer SPODI at the FRM-II research reactor (Garching, Munich, Germany) [18] using a wavelength of 1.548 Å. Synchrotron X-ray powder diffraction data on NET were recorded in Debye Scherrer geometry using image plate detector at the B2 instrument at HASYLAB/DESY (Hamburg, Germany) [19]. Data were collected in 0.004° 2θ steps over the angular range 5–60° using a wavelength of 0.5 Å. Sample was filled in a quartz capillary and rotated during the measurement. Structural parameters were refined by Rietveld method using the program FULLPROF [20]. A pseudo-Voigt profile shape has been chosen to model the Bragg peaks. Background was fitted using linear interpolation between data points.

3. Results and discussion

Figs. 1a–c show part of the neutron powder diffraction patterns of NLT, NTT and synchrotron X-ray powder diffraction pattern of NET. Two important features that needs to be carefully examined in a powder diffraction pattern of perovskite are: (i) splitting of the characteristic pseudocubic reflections and (ii) presence/absence of superlattice reflections. For NNT and NET the pseudocubic h 0 0 and *h h h* reflections are split suggesting the monoclinic distortion of cubic lattice. However, this monoclinic distortion is very special in the sense that two of its sides are equal ($a_p = b_p \neq c_p$, $\alpha_p = \beta_p = 90° \neq \gamma_p$). As a result, it is possible to choose the two perpendicular diagonals of the rhombus formed by $\mathbf{a_p}$ and $\mathbf{b_p}$ as lattice vectors of an orthorhombic cell. The space group of the orthorhombic structure can now be identified by considering the nature of superlattice reflections present in the powder patterns of NET and NTT. In the figures they have been labeled according to their origin. It is more convenient to identify the origin of the superlattice reflections after indexing the patterns on the basis of a doubled pseudo-cubic cell ($2a_p \times 2b_p \times 2c_p$). The indices in Fig. 1 correspond to such a cell settings. The main perovskite reflections have indices that are all-even (eee) integers. The superlattice reflections are characterized by indices with at least one odd integer. They fall under three categories: (i) all-odd (ooo) integer reflections, (ii) two-odd-one-even (ooe) integer reflections, and (iii) one-odd-two-even (oee) integer reflections. The first category appear due to out-of-phase (−) tilt of neighboring octahedra and are labeled as *R*-type since they refer to distortions of the cubic cell by a lattice instability of a soft R_{25} phonon in the cubic Brillouin zone. Following a similar argument, the second (i.e, ooe) and the third (i.e., oee) type of the superlattice reflections are labeled as *M* and *X*, respectively. The *X* reflections, however, are not independent and arise from the coupling of *R* and *M*-point distortions.

In view of Glazer's classification scheme [6,7] and the arguments discussed above, a combination of orthorhombic

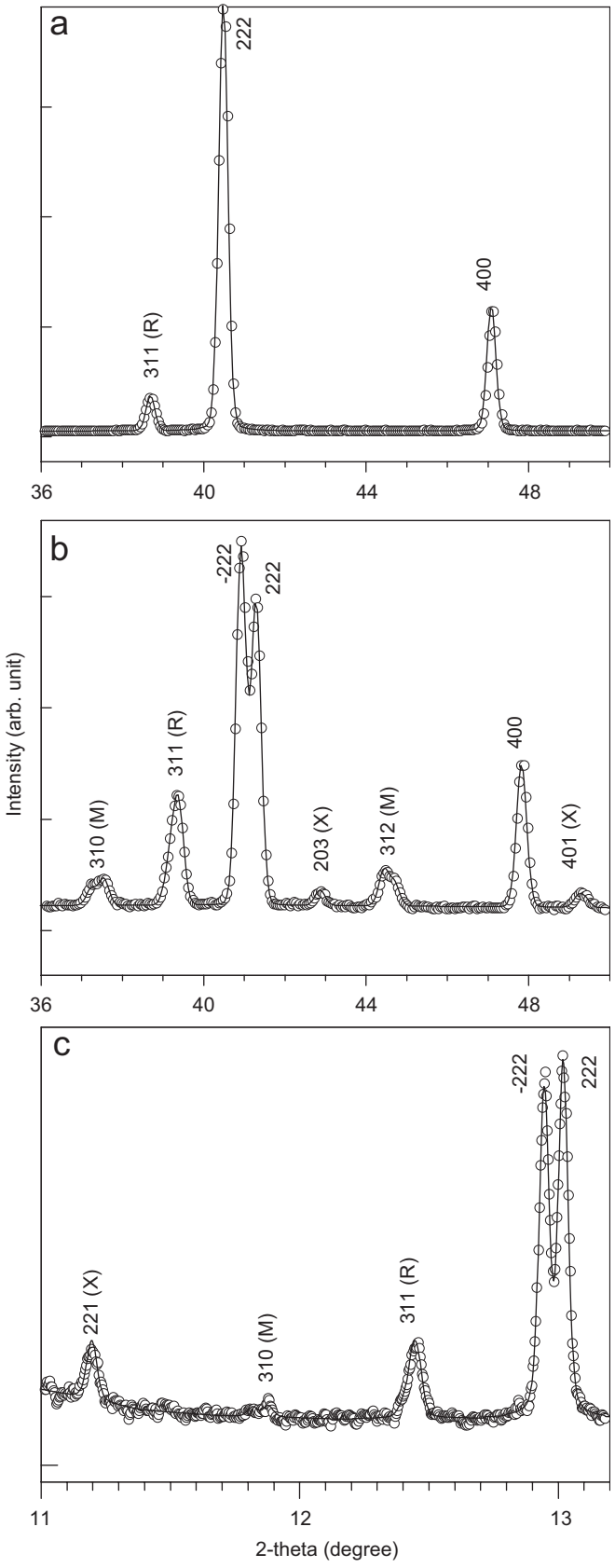

Fig. 1. Powder neutron diffraction patterns of (a) $Na_{1/2}La_{1/2}TiO_3$, (b) $Na_{1/2}Tb_{1/2}TiO_3$, and (c) synchrotron X-ray diffraction pattern of $Na_{1/2}Eu_{1/2}TiO_3$ in a limited 2θ range. The indices correspond to a doubled pseudocubic cell.

cell along with the presence of *R* and *M* types reflections unambiguously identifies the space group *Pbnm*, corresponding to the tilt system $a^-a^-c^+$, for both NET and NTT. Structure refinement of NET and NTT was therefore carried out using this structural model. For NTT, anisotropic atomic displacement parameters were refined for all the atoms. Keeping in mind the fact that we have used XRD data for NET, we refined anisotropic displacement parameters only for Na/Eu and Ti, and isotropic ones for the two oxygen atoms. A very good fit between the calculated and observed patterns for NET and NTT, shown in Fig. 2(a) and (b), confirms the correctness of the structural model (*Pbnm*) for both compounds. The refined structural parameters are listed in Table 1.

As mentioned above, earlier reports on NLT are not unanimous. However, since the diffraction pattern of the orthorhombic (*Pbnm*) structure, considered in Refs. [9,16,17], should have additional *M* type superlattice reflections in comparison to the patterns of the tetragonal (*I4/mcm*) [9] and rhombohedral ($R\bar{3}c$) structures, in principle there should be no ambiguity in the choice between the orthorhombic and the rhombohedral/tetragonal structures.

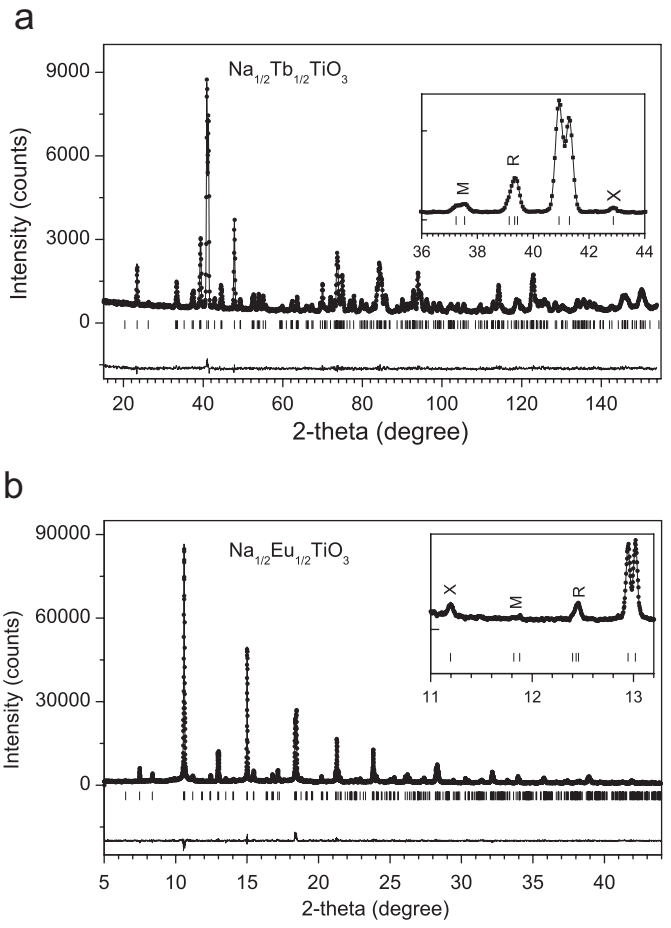

Fig. 2. Observed (open circles), calculated (continuous line) and difference (continuous line near the bottom) plots after the final cycle of refinement in the *Pbnm* space group. The vertical bars indicate positions of Bragg peaks. (a) $Na_{1/2}Tb_{1/2}TiO_3$ (NTT) and (b) $Na_{1/2}Eu_{1/2}TiO_3$ (NET).

Table 1
Refined structural parameters and R-factors of $Na_{1/2}La_{1/2}TiO_3$, $Na_{1/2}Tb_{1/2}TiO_3$ and $Na_{1/2}Eu_{1/2}TiO_3$

	$Na_{1/2}La_{1/2}TiO_3$			$Na_{1/2}Tb_{1/2}TiO_3$			$Na_{1/2}Eu_{1/2}TiO_3$		
	$R\bar{3}c$			*Pbnm*			*Pbnm*		
a, b, c (Å)	5.48099(6)	5.48099(6)	13.4092(3)	5.3645(1)	5.43498(1)	7.6361(2)	5.39338(8)	5.43903(8)	7.6625(1)
Na/Ln									
x/a, y/b, z/c	0	0	0.25	0.0067(5)	0.5362(3)	0.25	0.0065(2)	0.5317(1)	0.25
$u_{11}/u_{22}/u_{33}$	0.007(1)	0.007(1)	0.0016(2)	0.0080(8)	0.0092(6)	0.0020(3)	0.0009(3)	0.0024(3)	0.0041(2)
$u_{12}/u_{13}/u_{23}$	0.0035(5)	0	0	0.0018(6)	0	0	−0.0001(5)	0	0
Ti									
x/a, y/b, z/c	0	0	0	0	0	0	0	0	0
$u_{11}/u_{22}/u_{33}$	0.004(1)	0.004(1)	0.002(2)	0.005(1)	0.005(1)	0.0018(5)	0.0035(6)	0.0002(7)	0.0018(3)
$u_{12}/u_{13}/u_{23}$	0.002(7)	0	0	−0.0013(8)	−0.001(1)	0.0027(5)	−0.0002(13)	−0.0009(8)	−0.0015(3)
O1									
x/a, y/b, z/c	0.1272(6)	0.335(1)	0.0833	−0.0750(4)	−0.0184(4)	0.25	−0.071(1)	−0.0147(9)	0.25
$u_{11}/u_{22}/u_{33}$	0.0010(5)	0.0043(5)	0.0016(1)	0.0121(7)	0.0097(7)	0.0005(3)	0.003(1)	0.003(1)	0.003(1)
$u_{12}/u_{13}/u_{23}$	−0.0075(4)	0	0	0.0018(6)	0	0	0	0	0
O2									
x/a, y/b, z/c	—	—	—	0.2098(3)	0.2902(2)	0.0385(2)	0.2148(9)	0.2883(9)	0.0361(5)
$u_{11}/u_{22}/u_{33}$	—	—	—	0.0078(4)	0.0081(3)	0.0048(2)	0.003(1)	0.003(1)	0.003(1)
$u_{12}/u_{13}/u_{23}$	—	—	—	−0.0051(4)	0.0013(3)	−0.0013(3)	0	0	0
R_p, R_{wp}, χ^2	3.55	4.70	2.54	3.56	4.56	1.49	5.74	7.22	9.58

The ambiguity about the presence/absence of the *M* point reflections in these previous studies could be due to the fact that these authors used X-ray diffraction data for the structure analysis. In view of this, we collected neutron diffraction data on NLT with very good counting statistics (absolute count of the maximum peak ~45,000). The strict absence of any *M*-superlattice reflections in Fig. 1, clearly rules out the possibility of the orthorhombic (*Pbnm*) structure as a possible candidate among the competing structural models of NLT.

A perusal of the Glazer tilt system suggests that there are six possible space groups corresponding to only minus tilts: one in the tetragonal system (space group *I4/mcm*); one in the orthorhombic system (space group *Ibmm*); two in the monoclinic system (space groups *C2/m* and *C2/c*); one in the rhombohedral system (space group $R\bar{3}c$); and one in the triclinic system (space group $F\bar{1}$). The problem of identifying the correct crystal system is easy when the distortion of the cubic lattice is significantly large enough to observe splitting of the pseudocubic reflections. However, in contrast to NET and NTT, the Bragg peaks are not split in NLT, indicating very weak lattice distortion. We therefore, did not consider the lower symmetry space groups in the orthorhombic, monoclinic and triclinic systems, since they are subgroups of the remaining ones, i.e., *I4/mcm* and $R\bar{3}c$. Rietveld refinements were therefore compared for the latter space groups only. The rhombohedral structure consists of anti-phase rotated (tilt system $a^-a^-a^-$) octahedra about [111] pseudocubic axis. The asymmetric unit consists of one Na/La occupying the 6*a* site at (0,0,0.25), one Ti occupying the 6*b* site at (0,0,0) and one O occupying the 18*e* site at (0.5 + (δx), 0, 0.25). In our refinement we have, however, followed the convention of Megaw and Darlington [21] in describing the various positional coordinates. This description allows for direct determination of the magnitude of the tilt angle (ω) about the pseudocubic [111] axis using the relationship $\tan\omega = 4\sqrt{3}e$, where e is determined from the refined values of the *x* and *y* coordinates of oxygen, described as (1/6-2*e*-2*d*, 1/3-4*d*, 1/12). The asymmetric unit of the alternative competing tetragonal structure (*I4/mcm*), consists of one Na/La occupying the 4*b* site at (0, 0.5, 0.25), one Ti occupying the 4*c* site at (0,0,0), one oxygen (O1) occupying the 4*a* site at (0, 0, 0.25), and another oxygen (O2) occupying the 8*h* site at (0.25-δ, 0.25 + δ, 0.00).

Initially, Rietveld refinement with both the models was carried out using isotropic thermal parameters only. The fit with the tetragonal *I4/mcm* space group was found to be significantly inferior compared to that for $R\bar{3}c$. The goodness-of-fit χ^2 for the *I4/mcm* and $R\bar{3}c$ space groups are 5.46 and 2.91, respectively, clearly confirming the rhombohedral structure for NLT. The final structure refinement was carried out using anisotropic atomic displacement parameters for all atoms. Fig. 3 depicts the Rietveld plot of NLT after the final cycle of refinement. The refined structural parameters are given in Table 1. The reduced cell parameters a_r and c_r, obtained from the rhombohedral lattice parameters a_h and c_h through the relation $a_r = a_h/\sqrt{2}$, and $c_r = c_h/2\sqrt{3}$, are 3.875 Å and

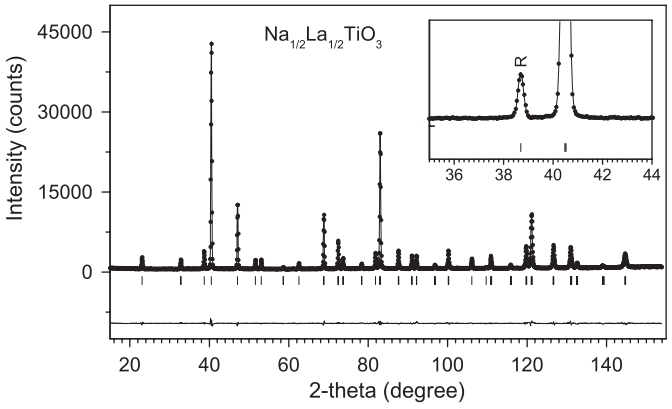

Fig. 3. Observed (open circles), calculated (continuous line), and difference (continuous line near the bottom) plots of $Na_{1/2}La_{1/2}TiO_3$ after refinement in the $R\bar{3}c$ space group. The vertical bars indicate positions of Bragg peaks.

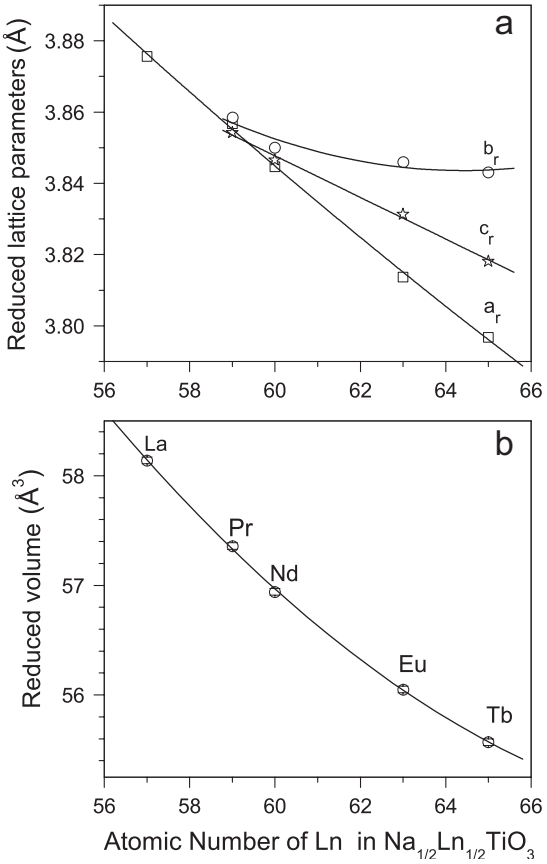

Fig. 4. Variation of (a) reduced perovskite lattice parameters and (b) reduced cell volume with atomic number of *Ln* in $Na_{1/2}Ln_{1/2}TiO_3$. The reduced lattice parameters (a_r, b_r, c_r) for the *Ln* = Pr, Nd, Eu and Tb were derived from their respective refined orthorhombic lattice parameters (a_o, b_o, c_o) using the relation: $a_r = a_o/\sqrt{2}$, $b_r = b_o/\sqrt{2}$ and $c_r = c_o/2$. The reduced cell parameter plotted for *Ln* = La was obtained using the relation $a_r = a_h/\sqrt{2}$, where a_h is the refined hexagonal a-parameter of this compound (see Table 1). The reduced volume corresponds to volume per formula unit of the compound.

3.871 Å, respectively. The small difference of 0.005 Å between the two parameters is a further proof of the weak lattice distortion in NLT.

In summary, of the various rare earth elements (*Ln*) in the series $Na_{1/2}Ln_{1/2}TiO_3$, only the La compound has $R\bar{3}c$ symmetry, and all others belong to *Pbnm* [14]. Fig. 4(a) depicts the variation of reduced lattice parameters of $Na_{1/2}Ln_{1/2}TiO_3$ as a function of Z of *Ln*. The values for NNT and NPT are taken from Ref. [14]. The *a*-parameter is most sensitive while the *b*-parameter is least sensitive to *Z*. The reduced cell volume exhibits a monotonic decrease with increasing the atomic number of *Ln* in $Na_{1/2}Ln_{1/2}TiO_3$ (see Fig. 4(b)). This decrease is obviously a feature related to lanthanide contraction of *Ln* with increasing *Z*. Fig. 5a depicts the variation of tilt angles with *Z*. For NLT the out-of-phase tilt angle is around the pseudocubic [111] direction. For the orthorhombic (*Pbnm*) structures, the in-phase (+) and out-of-phase tilt angles are around [001] and [110] pseudocubic axes, respectively, and their magnitudes were derived from the location of the equatorial oxygen O2 at $1/4-u$, $1/4+v$, w. The in-phase tilt angle (φ) about [001] pseudocubic axis is given by $\tan\varphi = 2(u+v)$, and the out-of-phase tilt angle (ψ) about the [110] pseudocubic axis is given by the relation: $\tan\psi = 4\sqrt{2}w$. For the orthorhombic structures, the magnitude of the in-phase and out-of-phase tilts increases with increasing *Z* (see Fig. 5a) and is consistent with the shrinking cell volume (cf. Fig. 4b). A consideration of tolerance factor in perovskite also predicts an increasing distortion with decreasing size of the *A* cations. Although the out-of-phase tilt angle in NLT (7.8° around the pseudocubic [111] axis) is considerably larger than that of NPT (4.5° about the [110] pseudocubic axis), the in-phase tilt angle of NPT (9.1°) is reasonably larger in magnitude. Thus, in the overall sense, NPT is more distorted than NLT.

The various Na/*Ln*–O, Ti–O bond distances, and Ti–O–Ti bond angles of $Na_{1/2}Ln_{1/2}TiO_3$ (*Ln* = La, Pr, Nd, Eu and Tb) are given in Table 2. The values for *Ln* = Pr, and Nd, were obtained using the coordinates given in Ref. [14]. The *A*-cation in the ABO_3 is surrounded by 12 neighboring O atoms at distances between 2.335(3)Å to 3.246(2) Å in NTT. The minimum scatter in the *A*–O bond lengths is found for NLT for which the *A*–O distances vary between 2.520 and 2.961 Å. For the orthorhombic structures, the *A*–O bond lengths can be classified into two categories: short bonds corresponding to distances less than 2.8 Å, and long bonds corresponding to distances greater than 2.8 Å. For NPT there are six short and six long *A*–O bonds. For the remaining compounds in this series, there are eight short bonds. Furthermore, the difference between the mean values of the long and short bonds increases with increasing Z (see Fig. 5b). The variations in the Ti–O bond distances are comparatively small. The Ti–O bond lengths vary around 1.95 Å by ±0.02 Å through out the series. The average bond distance shows a weak increase with increasing Z of *Ln* (see Fig. 5c). The Ti–O–Ti bond angles show an increasing deviation from 180° with increasing Z value of *Ln* (Fig. 5d) which is consistent with the increasing magnitude of the octahedral tilt angles in the series with increasing Z.

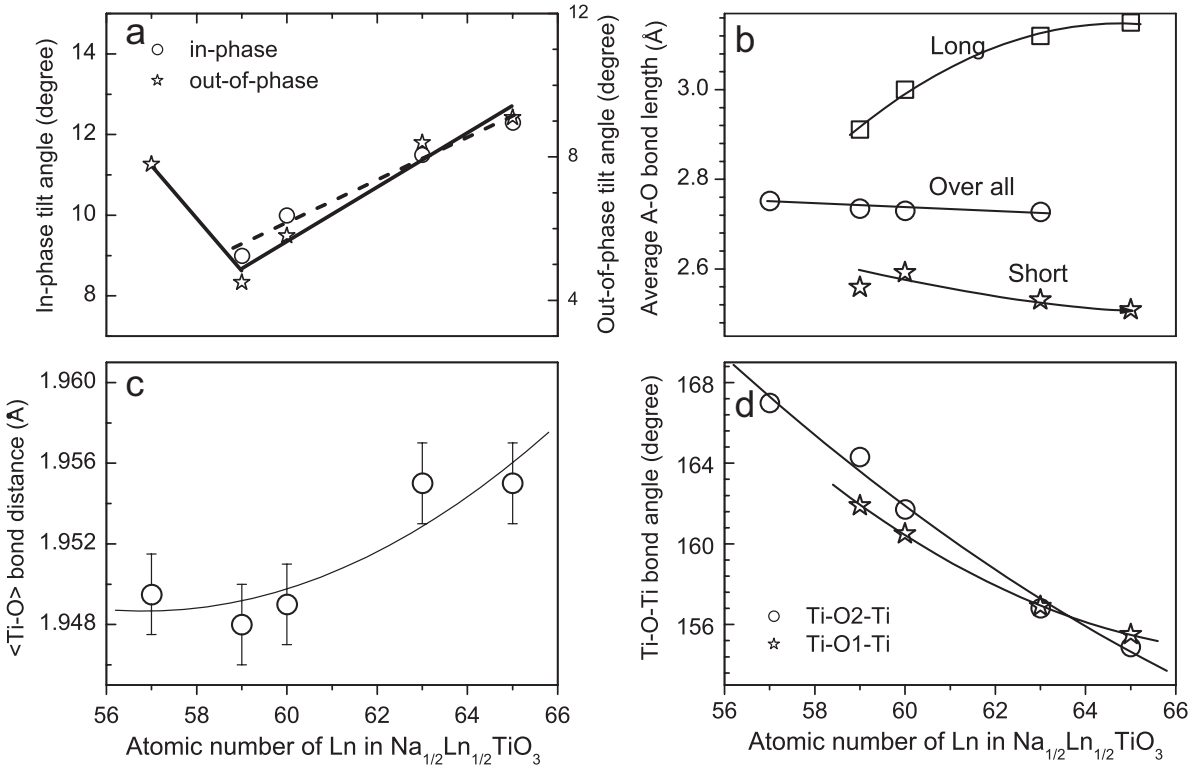

Fig. 5. Variation of (a) octahedral tilt angles (see text), (b) mean Na/*Ln*–O bond distances, (c) mean Ti–O bond distance, and (d) Ti–O–Ti bond angles with atomic number of *Ln* in $Na_{1/2}Ln_{1/2}TiO_3$.

Table 2
Bond length (in angstrom) and bond angle (in degree) of $Na_{1/2}Ln_{1/2}TiO_3$

	$R\bar{3}c$		*Pbnm*			
	NLT		NPT[a]	NNT[a]	NET	NTT
A–O ×3	2.752(4)	*A*–O1 ×1	2.803(9)	2.849(6)	3.005(5)	3.046(3)
A–O ×3	2.742(4)	*A*–O1 ×1	2.709(9)	2.635(6)	2.499(6)	2.460(3)
A–O ×3	2.520(4)	*A*–O1 ×1	2.503(17)	2.395(11)	2.364(6)	2.335(3)
A–O ×3	2.961(4)	*A*–O1 ×1	2.952(17)	3.046(11)	3.054(6)	3.063(3)
⟨*A*–O⟩	2.752	*A*–O2 ×2	2.441(9)	2.446(6)	2.388(5)	2.363(3)
		A–O2 ×2	3.045(10)	3.062(6)	3.211(5)	3.246(3)
		A–O2 ×2	2.631(10)	2.667(7)	2.626(5)	2.612(2)
		A–O2 ×2	2.811(9)	2.743(6)	2.680(4)	2.663(2)
		⟨*A*–O⟩	2.735	2.730	2.727	2.722
B–O ×3	1.956(6)	*B*–O1 ×2	1.9513(7)	1.9514(8)	1.9552(12)	1.9536(5)
B–O ×3	1.944(6)	*B*–O2 ×2	1.958(4)	1.945(2)	1.970(5)	1.960(1)
⟨*B*–O⟩	1.949	*B*–O2 ×2	1.936(4)	1.952(2)	1.939(5)	1.952(1)
		⟨*B*–O⟩	1.948	1.949	1.955	1.955
∠Ti–O–Ti	166.99(3)	∠Ti–O1–Ti	161.93(3)	160.50(3)	156.91(5)	155.46(2)
		∠Ti–O2–Ti	164.3(2)	161.7(1)	156.8(2)	154.89(2)

[a]The values are calculated using coordinates given in Ref. [14].

4. Conclusions

We have successfully refined the structures of three compounds in the series $Na_{1/2}Ln_{1/2}TiO_3$ (*Ln*: La, Eu and Tb). The compounds with *Ln* = Eu and Tb exhibit orthorhombic structures in space group *Pbnm*. The ambiguity regarding the structure of $Na_{1/2}La_{1/2}TiO_3$ has been resolved by careful analysis of neutron powder

diffraction data, and the correct space group is identified as $R\bar{3}c$. The various detailed structural parameters of these compounds are presented for the first time.

Acknowledgment

RR is grateful to Alexander von Humboldt Foundation for award of a fellowship.

References

[1] R.H. Mitchell, Perovskites: Modern and Ancient, Almaz Press, Ont., Canada, 2002.
[2] R.E. Newnham, Acta Cryst. A 54 (1998) 729–737.
[3] R.E. Newnham, G.R. Ruschau, J. Am. Ceram. Soc. 74 (1991) 463–480.
[4] G.-Q. Gong, C. Canedy, G. Xiao, J.Z. Sun, A. Gupta, W.J. Gallagher, Appl. Phys. Lett. 67 (1995) 1783–1785.
[5] M.A. Carpenter, E.K.H. Salje, Eur. J. Mineral. 10 (1998) 693–812.
[6] A.M. Glazer, Acta Crystallogr. B 28 (1972) 3384–3392.
[7] A.M. Glazer, Acta Crystallogr. A 31 (1975) 756–762.
[8] C.J. Howard, H.T. Stokes, Acta Crystallogr. A 61 (2005) 93–111.
[9] R.H. Mitchell, A.R. Chakhmouradian, P.M. Woodward, Phys. Chem. Miner. 27 (2000) 583–589.
[10] K.A. Muller, H. Burkard, Phys. Rev. B 19 (1979) 3593–3602.
[11] G.A. Samara, B. Morosin, Phys. Rev. B 8 (1973) 1256–1264.
[12] P. Sun, T. Hsuan, Y. Nakamura, J. Shan, Y. Inaguma, M. Itoh, Ferroelectrics 200 (1997) 93–107.
[13] Y.J. Shan, T. Nakamura, Y. Inaguma, M. Itoh, Sol. State Ion. 108 (1998) 123–128.
[14] R. Ranjan, A. Agrawal, A. Senyshyn, H. Boysen, J. Phys. Condens. Matter 18 (2006) L515–L522.
[15] R. Ranjan, A. Agrawal, A. Senyshyn, H. Boysen, J. Phys. Condens. Matter 18 (2006) 9679–9690.
[16] R.H. Mitchell, R. Chakhmouradian, J. Sol. State Chem. 138 (1998) 307–312.
[17] M.C. Knapp, P.M. Woodward, J. Sol. State Chem. 179 (2006) 1076–1085.
[18] R. Gilles, B. Krimmer, H. Boysen, H. Fuess, Appl. Phys. A 74 (2002) S148–S150.
[19] M. Knapp, C. Bähtz, H. Ehrenberg, H. Fuess, J. Synchr. Radiat. 11 (2004) 328–334.
[20] J. Rodrigues-Carvajal, FULLPROF. A Rietveld Refinement and Pattern Matching Analysis Program, Laboratoire Leon Brillouin (CEA-CNRS), France, 2000.
[21] H.D. Megaw, C.N.W. Darlington, Acta Cryst. A 31 (1975) 161–173.